Desalination and Water Treatment
www.deswater.com
doi: 10.1080/19443994.2015.1092890

57 (2016) 18475–18489
August

Taylor & Francis
Taylor & Francis Group

Equilibrium, kinetics, and mechanism of lead adsorption using zero-valent iron coated on diatomite

N. Pojananukij[a], K. Wantala[a,b,c], S. Neramittagapong[a,c], A. Neramittagapong[a,c,*]

[a]*Faculty of Engineering, Department of Chemical Engineering, KhonKaen University, KhonKaen 40002, Thailand, Tel. +664 336 2240; email: nusavadee@hotmail.com (N. Pojananukij), Tel./Fax: +664 336 2240, ext. 42; email: kitirote@kku.ac.th (K. Wantala), Tel. +664 336 2240; email: sutasineene@kku.ac.th (S. Neramittagapong), Tel./Fax: +664 336 2240; email: artner@kku.ac.th (A. Neramittagapong)*

[b]*Chemical Kinetics and Applied Catalysis Laboratory (CKCL), Faculty of Engineering, KhonKaen University, KhonKaen 40002, Thailand*

[c]*Research Center for Enviromental and Hazardous Substance Management (EHSM), Faculty of Engineering, KhonKaen University, KhonKaen 40002, Thailand*

Received 6 March 2015; Accepted 1 September 2015

ABSTRACT

The lead adsorption performances of zero-valent iron coated on diatomite (ZVI-D) were investigated. ZVI-D was prepared by impregnation of diatomite with iron sulfate solution, and followed by reducing with sodium borohydride. The zero-valent iron of ZVI-D was confirmed by XPS. The adsorption performances were tested in a batch reactor with an initial lead concentration in the range of 100–1,250 mg/L. It was found that a lead adsorption isotherm could be described by Langmuir equations with a maximum adsorption capacity of 158.73 mg/g at 298 K. The mean adsorption energy (*E*) of 54.78 kJ/mol was determined by using Dubinin–Radushkevich isotherm. The kinetics of Pb^{2+} adsorption was fitted with a pseudo-second-order model. From the thermodynamic study, it was found that the adsorption process was endothermic and spontaneous. An adsorption mechanism was proposed by using XPS data. Three steps of the adsorption were suggested, (i) Pb^{2+} ions were oxidized to Pb^0 on ZVI active sites, (ii)ferrous ions reacted with the Pb^{2+} to form FeOPbOH, PbO–Fe, PbO_2–Fe_2O_3, and PbO–FeOOH species on ZVI surface, and (iii) Pb^{2+} turned to PbO_2–Si, PbO–Si, $Pb(OH)_2$–Al, and PbO_2–Al_2O_3 on diatomite surface.

Keywords: Adsorption; Heavy metals; Kinetic adsorption isotherms; Thermodynamics; Adsorption mechanism

1. Introduction

An increasing level of toxic heavy metals, which have been discharged into the environment as industrial waste poses a severe threat to human health, and ecological systems [1–3]. Lead is one of the most widespread pollutants in the environment. It can cause anemia, nervous system disorders, reproductive system, liver, kidney diseases, and peripheral nervous system diseases [4]. Therefore, the World Health Organization (WHO) has set a drinking water standard for lead concentration of less than 0.01 mg/L [5]. Ion exchange, filtration, chemical precipitation, and adsorption are being used to remove heavy metals

*Corresponding author.

from wastewaters [6–9]. Among these methods, adsorption is a highly suitable and economical removal technique. One such process involves the use of nanoscale zero-valent iron (nZVI) for an *in situ* remediation of ground water and surface water as a suitable donor of electrons. It is a strong reducing agent which has low toxicity and is the most suitable for using in the environment [10,11]. A redox couple of Fe^0 and dissolved Fe^{2+} form has a standard reduction potential of 0.447 V [12]. Thus, it can be used as an adsorbent for removing heavy metal. It has also been confirmed that nZVI can remove metalloid and metallic contaminants [13]. In spite of the stated advantages of nZVI, in many cases, the nanoparticles agglomerate due to Van der Waals and magnetic attraction forces, which may lead to the loss of benefits associated with their natural high specific surface area. For this reason, the stability of nZVI on a support with good dispersion can result in steady or higher remediation capability. The dispersion of nZVI on the support can improve the adsorption capacity through preventing agglomeration of iron nanoparticles, and exposing highly reactive nanoparticles directly to the contaminants. The support materials, such as activated carbon, zeolite, bentonite, pillared clay, sand, and diatomite [11,14–17] are widely used. It has been reported that the porous structure of the matrix provides high hydraulic conductivity, which can yield faster heavy metal removal rates. Among the supports, synthesized zeolite shows a good adsorption performance, however, it has disadvantages due to high preparation costs. Since, diatomite ($SiO_2{\cdot}nH_2O$) is a kind of natural zeolite, soft and lightweight with porous structure, it provides many unique properties, such as high porosity (80–90% voids), high surface area and chemical inertness, and it is widely used as filter agents, catalyst carriers, building materials, and wastewater treatment agents (organic and inorganic) [16,18,19]. Thus, it has great potential for use as a support for nZVI. Generally, supported nZVI adsorbent has to be used immediately after preparation because it could be readily oxidized. In this work, a coating process has been chosen to stabilize a zero-valent iron on diatomite surface. Moreover, zero-valent iron coated on diatomite (ZVI-D) has not been used for the removal of Pb(II) ions from wastewater. At the same time, the understanding of mechanisms responsible for the adsorption of metal ions by the nZVI is still lacking due to the difficulty in identifying the adsorbed species on the surface of the adsorbent.

In this work, the main focuses are as follows: (i) synthesize and characterize ZVI-D by using BET–N_2 adsorption technique, scanning electron microscopy (SEM), X-ray diffraction (XRD), Fourier transform infrared (FTIR), and X-ray photoelectron spectroscope (XPS), (ii) study the kinetic adsorption isotherms, adsorption isotherm models, and thermodynamics, and (iii) study the mechanism of lead adsorption by ZVI-D. The results from this study can be used to evaluate the benefit of ZVI-D for heavy metal removal, in particular lead adsorption, at the field scale.

2. Materials and methods

2.1. Materials

The diatomite sample was acquired from the North of Thailand and was grated in a sphere mill until it had the size of 150 micron, which was used as a support for iron. It mainly consists of SiO_2 (79.76%), Al_2O_3 (9.61%), and Fe_2O_3 (2.49%), and has a specific surface area of 26.8 m^2/g. These samples were washed with distilled water three times to remove the contaminants, and dried in an oven at 110˚ for 24 h. Finally, they were stored in closed polyethylene bags for further use. All chemicals used in the experiments were analytical grade reagents; namely, lead(II) nitrate ($Pb(NO_3)_2$, Ajax Finechem; Australia), iron(III) sulfate ($FeSO_4{\cdot}7H_2O$, Ajax Finechem; Australia), sodium borohydride ($NaBH_4$, Rankem; India), ammonium hydroxide (NH_4OH, Panreac; Barcelona), and hydrogen chloride (HCl, RCL Labscan; Thailand), together with distilled water which was purified with a Millipore Milli-Q equipment (resistivity of 18 MΩ cm).

2.2. Preparation of ZVI-D_N

ZVI-D was synthesized by the reduction of ferrous ion and diatomite with sodium borohydride ($NaBH_4$). The reaction is given in Eq. (1):

$$2Fe^{2+} + 4BH_4^- + 2H_2O \rightarrow 2Fe^0 + 4BO_2^- + 2H_2 + 4H^+ \quad (1)$$

Firstly, the synthesized iron-oxide-coated diatomite (IOCD) was prepared by the method similar to that described in Yi-Fong Pan et al. [16] for coating iron oxide onto diatomite. A total of 20 g of diatomite was mixed with 100 ml of 2 M $FeSO_4$ solution. The mixture was covered and stirred for 30 min. Then, it was dried at 110˚C by heating. After being cooled to the room temperature, the solid was washed with deionized water until the solution was clear, and then the IOCD was dried at 110˚C in an oven for 24 h. The coating process was repeated three times. Secondly, 1 g of IOCD was reduced by dropping 50 ml of 0.1 M

$NaBH_4$ on it with the flow rate of 2 mL/min until the IOCD became black solid of Fe^0, indicating that it is a ZVI-D. Finally, ZVI-D, the mixture was sent into a 25 mL centrifugal tube and centrifuged with the rotating speed of 3,500 rpm for 5 min. The supernatant was removed and replaced by ethanol, followed by deionized water to remove any unreached residuals. The prepared ZVI-D samples are identified as ZVI-D_N, where N denotes the number of iron oxide coating times (one to three).

2.3. Characterization of ZVI-D_N

The specific surface area of a powder is determined using the Brunaeur, Emmett, and Teller method at 77 K on the ASAP 2010 analyzer (Micromeritics, USA). The surface morphology was characterized by scanning electron microscope (SEM, S-3000 N, Hitachi; Japan). The chemical composition and the crystallographic structure were determined by X-ray diffraction (XRD, Bruker D8 Advance; Germany) with CuαK radiation (40 kV, 40 mA). XRD patterns of ZVI-D over a wide range of angles (10–80˚, 2θ) were measured. Fourier transform infrared spectroscopy (FTIR, Bruker Tensor 27; USA) was used to identify the functional groups in a mixture over the spectral range of 400–4,000 cm^{-1}. The point of zero charge (pH_{pzc}) was determined by Zetasizer Nano Z (Malvern Instruments Ltd, UK). Measuring the ζ-potential in the range pH 1–12 and the solution pH was adjusted by adding 1 N HCl or 1 N NaOH. It is a concept relating to the phenomenon of adsorption, and it describes the condition when the electrical charge density on a surface is zero.

An XPS (AXIS Ultra Kratos Analytical Instrument; Manchester; UK) was used for the analysis of surface composition, the valence elements and distinction between different oxidation states of elements in ZVI-D_2 before and after lead ion adsorption within a depth of <10 nm. Survey and multiregional spectra were recorded for Pb 4f, O 1s, Fe $2p_{3/2}$, Fe $2p_{1/2}$, Si 2p, and Al 2p.

2.4. Batch experiments for adsorption of lead by ZVI-D_N

A stock solution 5,000 ppm of Pb^{2+} was prepared by dissolving 8 g of lead (II) nitrate ($Pb(NO_3)_2$) into distilled water and then diluted to 1,000 mL. Batch equilibrium studies were carried out by adding a fixed amount 1 g of the ZVI-D_N into 500-mL Erlenmeyer flasks with 100 mg/L of initial lead(II) concentrations, and the pH was carefully adjusted to 5 [2,15,20,21] by adding HCl or NH_4OH solution. The lead solutions were stirred using a mechanical magnetic stirrer with the speed of 160 rpm for 120 min.

Adsorption isotherms were obtained by varying the initial lead ion concentrations from 250 to 1,250 ppm in 250 mL vials with 0.5 g/L of the ZVI-D_2 at pH 5 and 30˚C. The samples were collected over a period of 120 min to quantify the initial and final Pb^{2+} concentrations. The suspensions were filtered with syringe Filter Nylon 0.45 μm membrane (Lubitech, Thailand). The pH of the solution was adjusted to acidic range to prevent the precipitation of heavy metals in the solution. The difference between the initial and the final lead concentrations of the suspension was recorded as the amount of lead adsorbed with atomic absorption spectroscopy (AAS, AAnalyst, Perkin Elmer, USA). The adsorption capacity, Q_e (mg/g), was determined as follows:

$$Q_e = \frac{(C_0 - C_e)}{M} V \quad (2)$$

where C_0 and C_e are the initial and equilibrium solution concentrations (mg/L), respectively; V is the volume of the solution (L); and M is the mass of the adsorbent (g).

3. Results and discussion

3.1. Characterization of ZVI-D_N

Diatomite was analyzed by XRF and found to be mainly composed of SiO_2 (79.761%), Al_2O_3 (9.618%), Fe oxide(2.496%), MgO (0.853%), K_2O (0.746%), CaO (0.160%), and TiO_2(0.147%). The X-ray powder diffraction results of diatomite and ZVI-D_N are presented in Fig. 1, the diffraction spectrogram indicates that the diatomite mainly consisted of silica (SiO_2) in quartz and tridymite phases [19]. The increased amounts of iron oxide resulted in the decrease in the major peak intensity of quartz band. It is interesting to note that the results of XRD revealed no peaks of Fe. This might be due to very good dispersion of Fe over the surface of diatomite.

The quantity of Fe in diatomite was determined by digesting 1 g of ZVI-D_N in 200 mL of deionized water and 5 mL of nitric acid, and then heating it up until the solution volume remained about 20 mL. Subsequently, the measurement of Fe was carried out by atomic absorption spectroscopy. The AAS results showed that the dosage of Fe in diatomite in a single iron coating was 2.87% by mass, 8.59% for a double iron coating and 9.3% for a triple iron coating. These results are similar to those of Wantala et al. [22]. It is worth noting that amount of Fe in the triple coating

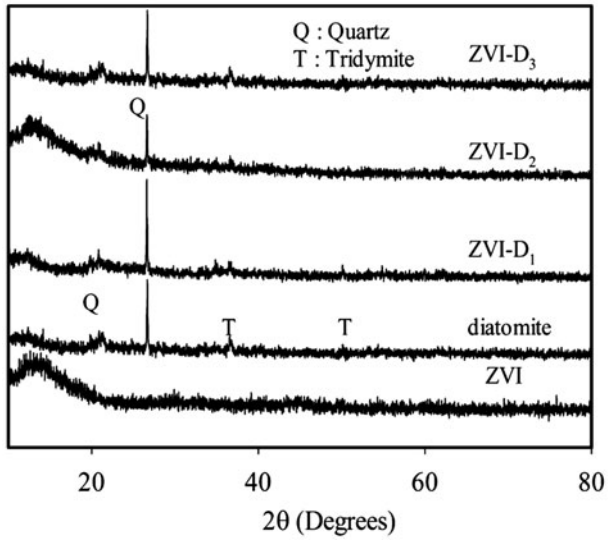

Fig. 1. XRD patterns of diatomite, ZVI, ZVI-D_1: single iron oxide coating, ZVI-D_2: double iron oxide coating and ZVI-D_3: triple iron oxide coating.

has not much increased than that of the double coating. This might be because the Fe was not able to fully insert into the porous structure of the diatomite but was deposited on the outer surface. So, the sum of Fe increased only slightly.

In this study, the specific surface area of diatomite and ZVI was 26.80 and 24.06 m^2/g, respectively, but the specific surface area of ZVI-D_1 decreased to 17.69 m^2/g, while the total pore volume decreased from 0.069 to 0.052 cm^3/g. In the same way, the surface area of ZVI-D_2 was reduced to 14.16 m^2/g, which is less than ZVI-D_1 because the amount of ZVI on diatomite has more volume and the total pore volume decreased to 0.050 cm^3/g because ZVI blocked the pore structure of diatomite [23]. In contrast with ZVI-D_1 and ZVI-D_2, the specific surface area and the total pore volume of ZVI-D_3 increased to 33.35 m^2/g and 0.075 cm^3/g, respectively. The reduction of both the specific surface area and the pore volume in the cases of ZVI-D_1 and ZVI-D2 can be easily explained with the help of SEM analysis as depicted in Fig. 2(a–c). The coating will reduce the pore volume, hence the specific surface area. Similarly, the increase in the specific surface area in case of ZVI-D_3 can be explained by Fig. 2(d). It was seen from the figure that the diatomite crumbled, thus the specific surface area increased.

The FT-IR spectrum of diatomite (figures not shown) shows the major adsorption bands at 3,695, 1,029, 796, 693, 551, and 412 cm^{-1}. The band at 3,695 cm^{-1} was ascribed to free silanol group (SiO–H) on the surface. The peaks at 1,029 and 412 cm^{-1} were ascribed to the asymmetric stretching modes of Si–O–Si bonds, and the peak at 796 cm^{-1} corresponded to SiO–H vibration [24,25]. Moreover, the FT-IR spectra of iron oxide-coated diatomite show the new adsorption peaks at 550 and 437 cm^{-1} corresponding to Fe–O stretches of Fe_2O_3 and Fe_3O_4, and the peak at 595 cm^{-1} may correspond to Fe–O stretches of Fe–O–Si and δ-FeOOH which could be confirmed by the peak at 447 cm^{-1} [26]. The peak of Fe_2O_3, Fe_3O_4, and δ-FeOOH showed that reduction with $NaBH_4$ to ZVI-D_n could easily take place since the binding bond of iron oxide on the diatomite was not strong, so $NaBH_4$ can be readily reactive.

3.2. Adsorption efficiency of lead by diatomite, ZVI, and ZVI-D_N

Fig. 3(a) shows the solution concentrations of Pb^{2+} as a function of reaction time for 1 g of ZVI-D_2, 1 g diatomite, and 0.085 g of ZVI in 500 mL of 100 ppm lead ion concentration at room temperature with the initial pH adjusted to 5; the solution pH increased to 7 during equilibration due to reaction of ZVI-D_2 and ZVI with the solution. The results indicate that the ZVI-D_2 effectively removed 97.36% of the lead ions from the aqueous solution, while ZVI and diatomite alone removed 88.84 and 27.81%, respectively. In addition, the adsorption capability of ZVI-D_2 was 1.13 and 3.69 times greater than ZVI and diatomite, respectively.

In this research, the initial pH of 5 was selected since some research suggested that the pH of 4–6 could remove lead ions up to 94% [26,27]. In the case of pH < 7.0, the main species was Pb^{2+} and the removal of Pb^{2+} was mainly achieved via adsorption reaction. The adsorption of Pb^{2+} can be attributed to the ion exchange between Pb^{2+} and H^+/Si^{2+} on the surface. While the predominant species at pH 7.0–10.0 were $Pb(OH)^+$ and $Pb(OH)_2$, at pH > 10.0, the main species were $Pb(OH)_3^-$ resulting in the decrease of lead ions adsorption onto ZVI-D_2 as a result of the competition between OH^- and $Pb(OH)_3^-$, and the precipitation began to occur in the solution at pH of Pb (II) ~ 8.7 [18]. In addition, in this study, the pH_{pzc} values of the diatomite and ZVI were 1.0 and 6.4, respectively, hence the pH_{pzc} values of ZVI-D_N were expected to be less than 6.4. Since, the pH of solution was greater than pH_{pzc} of ZVI-D_N, therefore, the adsorbent surface was negative. There was an electrostatic attraction between the negatively charged adsorbent surface and the lead ions, therefore lead ions were well adsorbed. On the other hand, if the pH of the solution is lower than pH_{pzc}, the charge on the

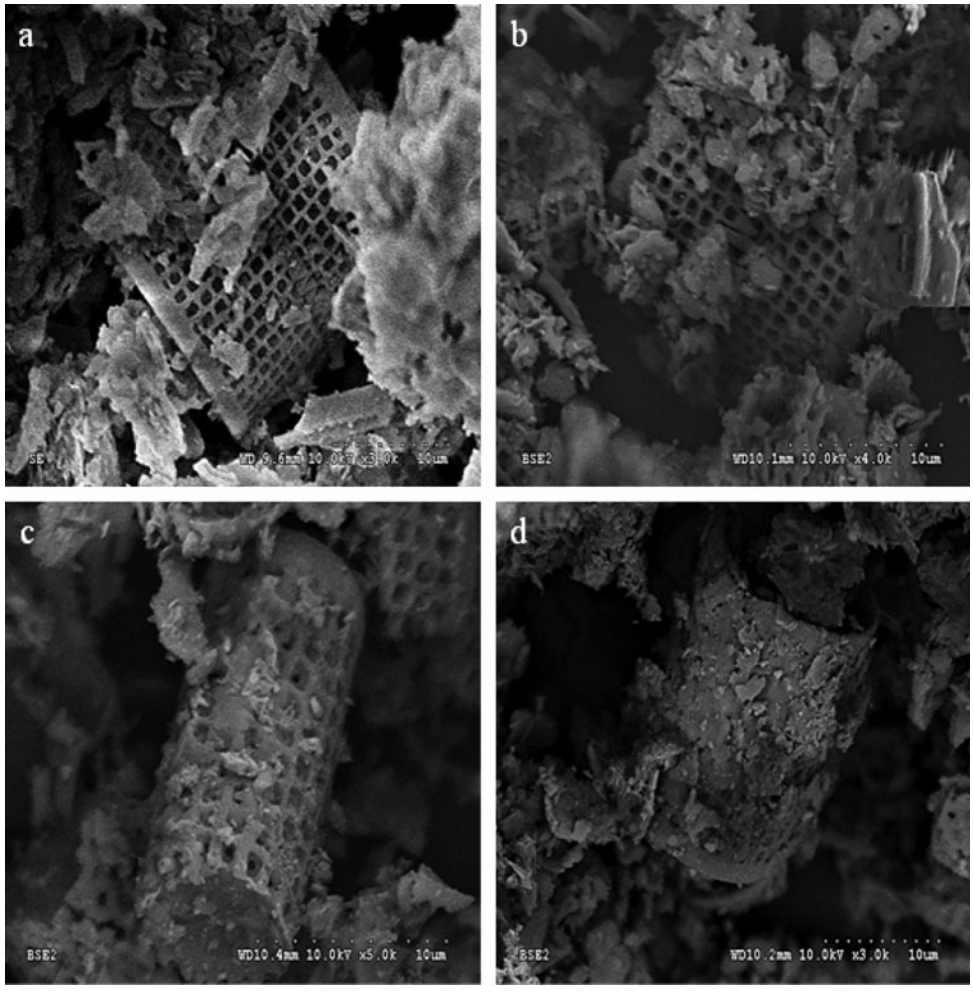

Fig. 2. Scanning electron microphotograph of (a) diatomite, (b) ZVI-D_1, (c) ZVI-D_2, and (d) ZVI-D_3.

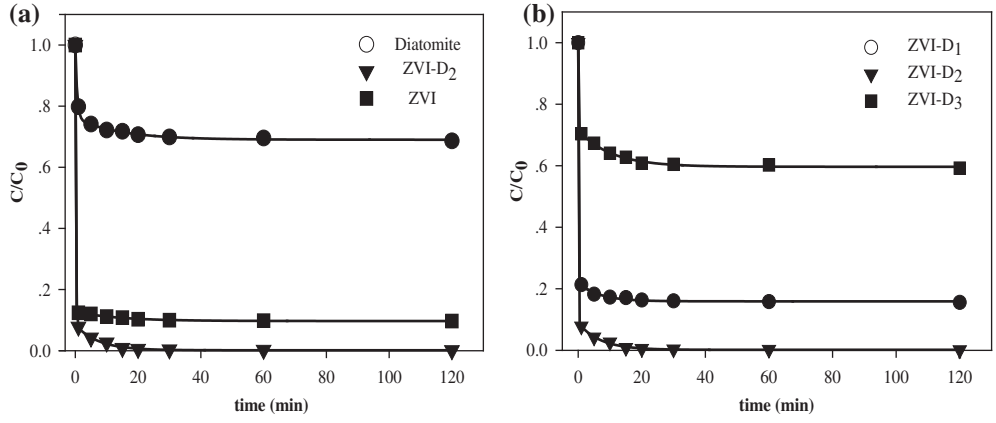

Fig. 3. Efficiency adsorption of lead by (a) Diatomite, ZVI, and ZVI-D_2 and (b) ZVI-D_1, ZVI-D_2, and ZVI-D_3 at 100 mg/L of initial lead concentration, pH 5 of initial pH and 30˚C.

adsorbent surface will be positive. There will be an electrostatic repulsion between the positively charged adsorbent surface and the lead ions, in which lead ion adsorption was lower [28].

The removal rate of lead by using ZVI-D_2 was more effective than using diatomite and ZVI as illustrated in Fig. 3(a). As a support material, diatomite would stabilize and disperse ZVI as well as prevent ZVI from aggregation. Better effectiveness of ZVI-D_2 is attributed to the capacities of both diatomite and ZVI in adsorbing lead. Therefore, the support increased the reactivity of ZVI even though ZVI-D_2 had a lower surface area than ZVI. In other words, the roles of diatomite and ZVI are complementary to each other. The removal of lead in the solution by ZVI can be explained by Eq. (3) [25].

$$2Fe^0 + 3Pb_2^+ + 4H_2O \rightarrow 3Pb^0 + 2FeOOH + 2H^+ \quad (3)$$

In the case of diatomite, adsorption occurs because of the different charges on the diatomite and the lead at pH < 7.0 [18]. Lead ions can also be adsorbed by the silanol groups (Si–OH) of diatomite. This process can be represented as Eqs. (4) and (5) [29]:

$$Si\text{–}OH + Pb^{2+} \leftrightarrow Si\text{–}OPb^+ + H^+ \quad (4)$$

$$2Si\text{–}OH + Pb^{2+} \rightarrow (Si\text{–}O)_2Pb + 2H^+ \quad (5)$$

For the case of ZVI-D, it has been reported that the occurrence of iron oxide on the surface of diatomite leads to the adhesive bonds of lead and iron oxides becoming $FeOHPb^{2+}$ complex dominantly at pH < 5.5 [30]. A study on the number of coatings of iron oxide on the diatomite was performed to determine the effectiveness of lead removal. It was found that ZVI-D_1, ZVI-D_2, and ZVI-D_3 removed 83.66, 99.45, and 39.17% of lead, respectively, as shown in Fig. 3(b). It is seen that ZVI-D_2 is the most effective. As previously explained, the specific surface area of ZVI-D_2 is less than that of ZVI-D_1 because the pores of diatomite were blocked by the loaded ZVI [31]. However, ZVI-D_2 was more effective because of greater mass of iron. Even though the specific surface area and iron loading in the case of ZVI-D_3 were greater than the others, it was the least effective. This is thought to be due to less specific surface area of iron on the diatomite (over coating).

A study of initial concentration of lead ions from 250 to 1,250 ppm was also conducted, and it was found that the adsorption rate increased sharply in the first 5 min and reached equilibrium in 30 min. It was also discovered that the adsorption capacities were independent of initial lead ion concentrations as shown in Fig. 4(a).

3.3. Adsorption isotherm

In this study, the equilibrium data for the adsorption of lead with ZVI-D_2 were examined by the Langmuir, Freundlich, and Dubinin–Radushkevich (D–R) isotherm models.

The linear form of Langmuir isotherm equation is given as:

$$\frac{C_e}{q_e} = \frac{C_e}{q_m} + \frac{1}{q_m K_L} \quad (6)$$

where K_L is the Langmuir adsorption constant (L/mg), q_e is the adsorption capacity in equilibrium (mg/g), q_{max} is the maximum concentration retained by the adsorbent (mg/g), and C_e is the solute concentration at equilibrium (mg/L). From the linear plot of C_e/q_e vs. C_e (Fig. 4(b)), the maximum adsorption capacity was determined as 158.73 mg/g. It was found that the maximum adsorption capacity in this study has a greater value than that of other researches using raw bentonite, kaolin and activated carbon [32], and untreated diatomite and Mn–diatomite as adsorbents [33].

The necessary characteristics of the Langmuir isotherms can be depicted in terms of a dimensionless factor or equilibrium parameter, R_L, as given by the equation:

$$R_L = \frac{1}{1 + K_L C_0} \quad (7)$$

where C_0 is the initial concentration of the adsorbate and K_L is the Langmuir constant. The R_L value indicates the shape of the isotherm. Considering the R_L value, adsorption can be unfavorable ($R_L > 0$), linear ($R_L = 1$), favorable ($0 < R_L < 1$), or irreversible ($R_L = 0$) [34,35]. In our case, the R_L value is 0.0018–0.0096. It is confirmed that the ZVI-D_2 is suitable for adsorbing lead ions for the initial concentration of 250–1,250 ppm.

The Freundlich isotherm model is shown below in its linear form:

$$\log q_e = \log K_F + \frac{1}{n} \log C_e \quad (8)$$

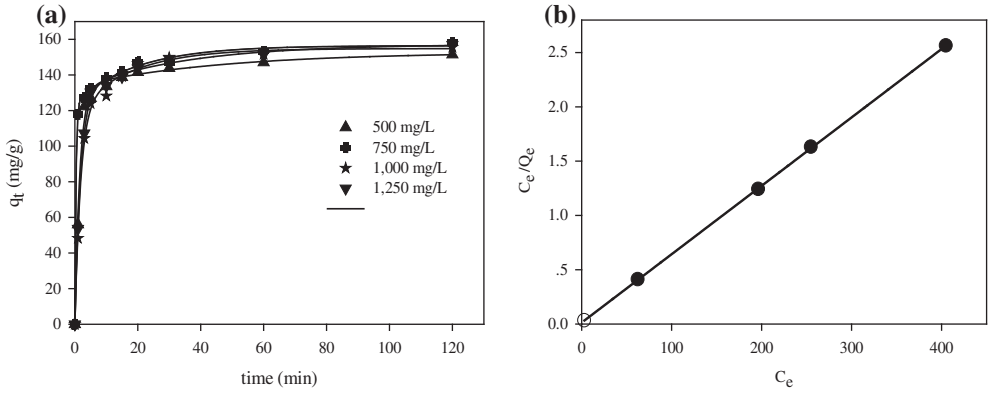

Fig. 4. (a) Effect of contact time per adsorption capacity for lead ion on ZVI-D_2 and (b) Adsorption isotherm models for Pb(II) ion on ZVI-D_2 at 298 K of Langmuir isotherm.

where K_F ((μg/g) (L/μg)$^{1/n}$) is the Freundlich constant and n is the adsorption intensity. These parameters are determined from a plot of log q_e vs. log C_e. The value of n implies the favorability of the adsorption process. The interpreter, $1/n$, gives an indication of the favorability of adsorption. Values of $n > 1$ represent favorable adsorption condition [36]. Based on this paper, it is shown that the value of n is equal to 11.123, which is greater than 1 meaning that it is chemisorption. There was a strong absorption between the adsorbate and adsorbent. The large value of n suggests that the adsorption capacity is weakly proportional to lead concentration in the solution.

The D–R adsorption isotherm model predicts the energy of adsorption per unit of adsorbate and a maximum adsorption capacity for the adsorbent. A linear form of D–R isotherm is:

$$\ln q_e = \ln q_d - \beta\varepsilon^2 \tag{9}$$

where q_d is the D–R monolayer capacity (mg/g), β is a constant related to adsorption energy, and ε is the Polanyi potential which is related to the equilibrium concentration as follows:

$$\varepsilon = \frac{RT}{M} \ln\left(1 + \frac{1}{C_e}\right) \tag{10}$$

where R is the gas constant (8.314 J/mol K), M is the molecular weight of the adsorbate, T is the absolute temperature, and C_e is the equilibrium concentration of the solute (mol/L). The mean adsorption energy, E (kJ/mol) is given by:

$$E = \frac{1}{\sqrt{2\beta}} \tag{11}$$

The adsorption energy provides information with regard to the physical and chemical characteristics of adsorption. When the magnitude of E is greater than 8 kJ/mol, the adsorption process follows that of the chemical adsorption, while for the values of $E < 8$ kJ/mol suggests that the adsorption process is the physical adsorption [24,37]. The energy value obtained in this research is 54.78 kJ/mol, indicating that the process is chemical adsorption. These results suggest that the Langmuir isotherm model should provide the best fit to the adsorption data than the other isotherm equations as shown in Table 1.

A comparison of the maximum adsorption capacity of ZVI-D_2 for Pb^{2+} with those of various adsorbents conducted within a similar concentration range is displayed in Table 2. The results show that the adsorption of Pb^{2+} onto ZVI-D_2 in this study was the greatest when compared with other researches.

3.4. Kinetic adsorption isotherms

The above reaction mechanism can be obtained from the kinetic adsorption and adsorption isotherms. The study of kinetic adsorption isotherms can be greatly beneficial to determine the information about the mechanism of adsorption and the efficiency of the adsorbents for the removal of pollutants. In this study, the adsorption data of ZVI-D_2 were fitted by three kinetic models, including the pseudo-first-order, the pseudo-second-order and the intra-particle diffusion models, to determine the best-fit kinetic adsorption isotherms. First, the kinetics of adsorption was analyzed by the pseudo-first-order kinetic model [32] which could be represented by the following equation:

$$\log(q_e - q_t) = \log q_e - \frac{k_1}{2.303} t \tag{12}$$

Table 1
Adsorption isotherm parameters for lead ion adsorption onto ZVI-D_2

Langmuir	Value	Freundlich	Value	Dubinin–Radushkevich	Value
q_m (mg/g)	158.73	n	11.12	E (kJ/mol)	54.78
K_L (L/mg)	0.488	K_F ((μg/g) (L/μg)$^{1/n}$)	96.805	K_D	0.00016
R^2	0.999	R^2	0.924	R^2	0.932

Table 2
Comparison of the maximum adsorption capacity of lead ion onto other adsorbents

Adsorbent	Concentration rate (ppm)	Model	Adsorption capacity (mg/g)	Refs.
Zero-valent ion-coated diatomite	250–1,250	Langmuir	158.73	This work
Diatomite	6–32	Freundlich	47.64	[18]
Diatomite	10–500	Freundlich	25.01	[28]
Pine cone	100	Langmuir	27.53	[21]
Montmorillonite–Illite	100–200	Langmuir–Freundlich	52.00	[29]
Mn–diatomite	200	Langmuir	99.00	[33]
Expanded perlite	10–400	Langmuir	13.39	[37]
Valonia tannin resin	20–120	Langmuir	53.19	[40]
Iron oxide-coated bentonite	2–10	Langmuir	22.20	[20]

where q_e is the amount of the solute adsorbed (mg/g) at equilibrium, q_t is the amount of the solute adsorbed (mg/g) at time, t (min), and k_1 (min^{-1}) is the rate constant of pseudo-first-order adsorption which is obtained from the slope of the linear plot of log $(q_e - q_t)$ vs. t (Fig. 5(a)). The R^2 values of the pseudo-first-order kinetic model obtained were lower than those of the pseudo-second-order kinetic model, and the $q_{e,cal}$ values of the pseudo-first-order kinetic model did not conform the experimental values as shown in Table 3. This indicates that the adsorption of lead by ZVI-D_2 did not follow the pseudo-first-order kinetics. Similar results were found for the adsorption of lead ions onto various adsorbents by several authors [21,32].

The pseudo-second-order rate expression representing the chemisorption kinetics in the liquid solutions [38] is linearly expressed as:

$$\frac{t}{q_t} = \frac{1}{k_2 q_e^2} + \frac{1}{q_e} t \tag{13}$$

The pseudo-second-order rate constants were determined experimentally by plotting t/q against t (Fig. 5(b)), where q_e and q_t are the amounts of solute adsorbed (mg/g) at equilibrium and time (t), respectively; and k_2 is the rate constant of pseudo-second-order adsorption (g/mg min). The initial adsorption rate, h (mg/g min), can be defined as:

$$h = k_2 q_e^2 \tag{14}$$

A linear plot is obtained with R^2 value of 0.999 at all the concentrations studied, thus indicating that the mechanisms of the adsorption of lead ions by ZVI-D_2, in which the predominant process was chemisorption, involving the absorption of the electrons on the surface of the adsorbent (mass transfer). Chemisorption may customarily absorb only one layer of molecules on the surface. The data indicated that the rate constant of adsorption (k_2) decreased when the initial lead concentration increased from 500 to 1,250 ppm, as seen in Table 3.

The different concentrations of adsorption with time could be used to appraise the function of diffusion in the adsorption process. The intra-particle diffusion rate constant (k_i) was given by Eq. (15) [38]:

$$q_t = k_i t^{1/2} \tag{15}$$

where k_i is the intra-particle diffusion rate constant (mmol/g min$^{1/2}$) obtained from a linear plot of q_t vs. $t^{1/2}$ (Fig. 5(c)). The rate of absorption depends on the size of adsorbate molecule or ion, the porous nature of adsorbent, the concentration of the adsorbate and the pore-size distribution of the adsorbent, and degree of mixing [39]. The adsorption process is considered to comprise three steps, one of which can be the

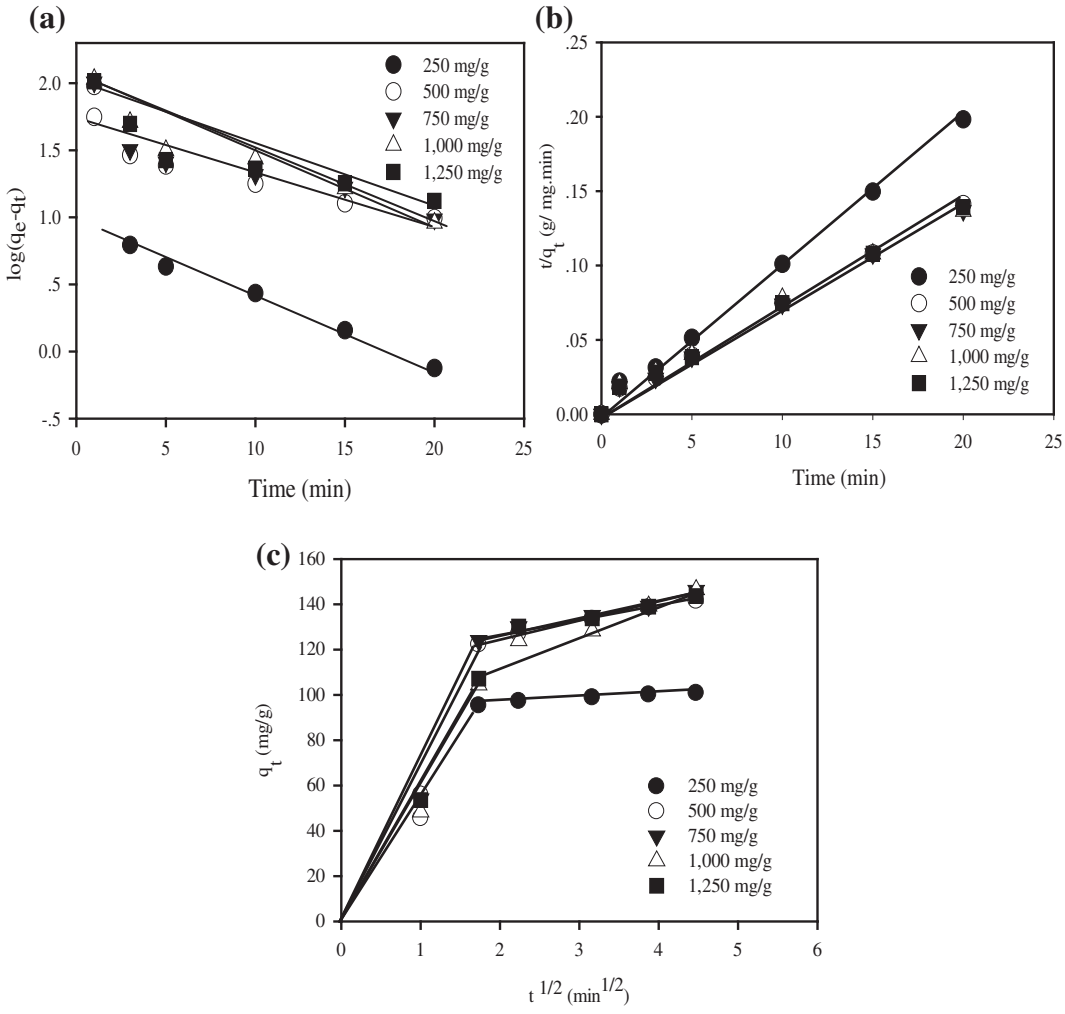

Fig. 5. Kinetic adsorption isotherm plots (a) Pseudo-first-order kinetics model, (b) Pseudo-second-order kinetics model, and (c) Intra-particle diffusion kinetics model of lead adsorption on ZVI-D_2 at 30°C.

Table 3
Kinetic adsorption model for lead ion adsorption onto ZVI-D_2 at the different concentrations

C_0 (mg/L)	500	750	1,000	1,250
$q_{e,exp}$ (mg/g)	151.44	155.86	155.56	156.92
Pseudo-first-order kinetic				
$q_{e,cal}$ (mg/g)	249.45	313.07	644.41	428.41
$k_1 \times 10^{-2}$ (L/min)	3.37	1.78	2.10	1.71
R^2	0.776	0.780	0.912	0.801
Pseudo-second-order kinetic				
$q_{e,cal}$ (mg/g)	149.25	153.84	158.73	166.67
$k_2 \times 10^{-3}$ (g/mg min)	5.99	5.15	3.31	4.54
R^2	0.997	0.997	0.996	0.998
Intra-particle diffusion				
k_i (mmol mg $min^{1/2}$)	11.68	20.42	23.946	21.885
R^2	0.506	0.637	0.785	0.728

rate-controlling step: (i) mass transfer across the external boundary layer film of liquid surrounding the outside of the particle; (ii) adsorption at a site on the surface and the energy depending on the binding process, this step is often assumed to be rapid; (iii) diffusion of the adsorbate molecules to an adsorption site either by a pore diffusion process through the liquid-filled pores or by a solid surface diffusion mechanism [38,40–42]. Since the adsorption step is very rapid, it is assumed that it does not influence the overall kinetics. The overall rate of adsorption process, therefore, will be controlled by either surface diffusion or intra-particle diffusion.

According to this model, a plot of q_t vs. $t^{1/2}$ should be linear when the adsorption process is involved in the intra-particle diffusion. If the plot passes through the origin, the intra-particle diffusion may totally be the rate-controlling step. If it does not

Table 4
Values of thermodynamic parameters for the lead ion adsorption onto ZVI-D_2

C_0 (ppm)	ΔH° (kJ/mol)	ΔS° (J/mol K)	ΔG° (kJ/mol)			
			303.15 K	313.15 K	323.15 K	333.15 K
300	16.34	68.38	−4.38	−5.06	−5.74	−6.43
400	15.26	61.44	−3.35	−3.97	−4.58	−5.19
500	17.15	64.00	−2.25	−2.88	−3.52	−4.16
600	47.11	155.37	−0.010	−1.54	−3.09	−4.65

pass through the origin, the boundary-layer diffusion controls the adsorption to some degree and the intra-particle diffusion is not the rate-controlling step totally, but the other processes may control the rate of adsorption [43]. It can be concluded from the multi-linear plots that more than one process controls the rate of adsorption, but only one is rate limiting. It is suggested from Fig. 5(c) that adsorption occurs in three parts. The external surface adsorption (part 1) is completed within 5 min, then the part of intra-particle or pore diffusion is rate limiting (part 2), from 5 to 30 min. At last, the final equilibrium adsorption (part 3) starts after 30 min. The lead ions are slowly transported through intra-particle diffusion into the particles, and finally maintained in the micro-pores [40]. While the values of R^2 obtained from the plots of intra-particle diffusion kinetics were lower than those of the pseudo-second-order model (Table 3), this model indicates that the adsorption of lead ions onto ZVI-D_2 may be followed by an intra-particle diffusion model up to 30 min. This suggests that the lead-ZVI-D_2 adsorption system belongs to the second-order equation, based on the assumption that the rate-limiting step may be intra-particle diffusion, film diffusion, and chemisorption involving valence forces through sharing or exchange of electrons between ZVI-D_2 and lead, which is similar to the absorption of lead on montmorillonite–illite-type clay, which was controlled by both intra-particle diffusion and film diffusion [29].

All kinetic data for the adsorption of lead by ZVI-D_2, calculated from the related plots, are summarized in Table 3. Comparison of the R^2 values for different models suggests that the pseudo-second-order kinetics fits best due to its highest value ($R^2 = 0.999$). But the pseudo-first-order and the intra-particle diffusion poorly fit the experimental data for the adsorption of lead. This suggests that the ZVI-D_2-Pb adsorption system is the second-order kinetics; based on the assumption that the rate-limiting step may be chemisorption involving valence forces through the exchange of electrons between ZVI-D_2 and lead ions.

3.5. Thermodynamic study

Thermodynamic parameters, including Gibbs free energy change (ΔG°), enthalpy change (ΔH°), and entropy change (ΔS°) for the adsorption process were obtained from the experiments carried out at different temperatures using the following Eq. (16) [43]:

$$\Delta G^\circ = -RT \ln K_L \tag{16}$$

where R is the universal gas constant (8.314 J/mol K), T is the temperature (K), and K_L value was calculated using the following Eq. (17):

$$K_L = \frac{q_e}{C_e} \tag{17}$$

where q_e and C_e are the equilibrium concentrations of lead ions on the ZVI-D_2 (mg/g) and in the solution (mg/L), respectively.

The enthalpy change (ΔH°) and entropy change (ΔS°) of the adsorption were estimated from the following equation:

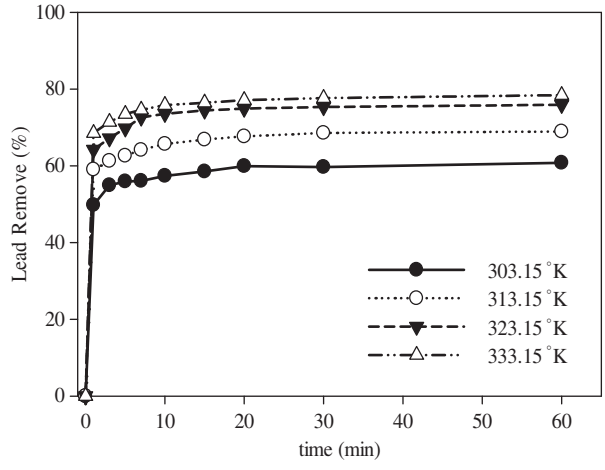

Fig. 6. Effect of temperature on the adsorption thermodynamic of lead ion by ZVI-D_2 at 400 mg/L: initial concentration, 1 g/L: ZVI-D_2 and pH 5.

$$\ln K_L = \frac{\Delta S^\circ}{R} - \frac{\Delta H^\circ}{RT} \quad (18)$$

The values of enthalpy and entropy changes were calculated from the slope and intercept of the plot of $\ln K_L$ vs. $1/T$ (Fig. 7). The enthalpy (ΔH°) and entropy (ΔS°) can be obtained from the slope and the intercept of a Van't Hoff equation of (ΔG°) vs.:

$$\Delta G^\circ = \Delta H^\circ - T\Delta S^\circ \quad (19)$$

where ΔG° is the Gibbs free energy change (J), R is the universal gas constant (8.314 J/mol K), and T is the absolute temperature (K).

The thermodynamic parameters obtained are shown in Table 4. An increase in temperature resulted in an interesting rate of lead adsorption [44],

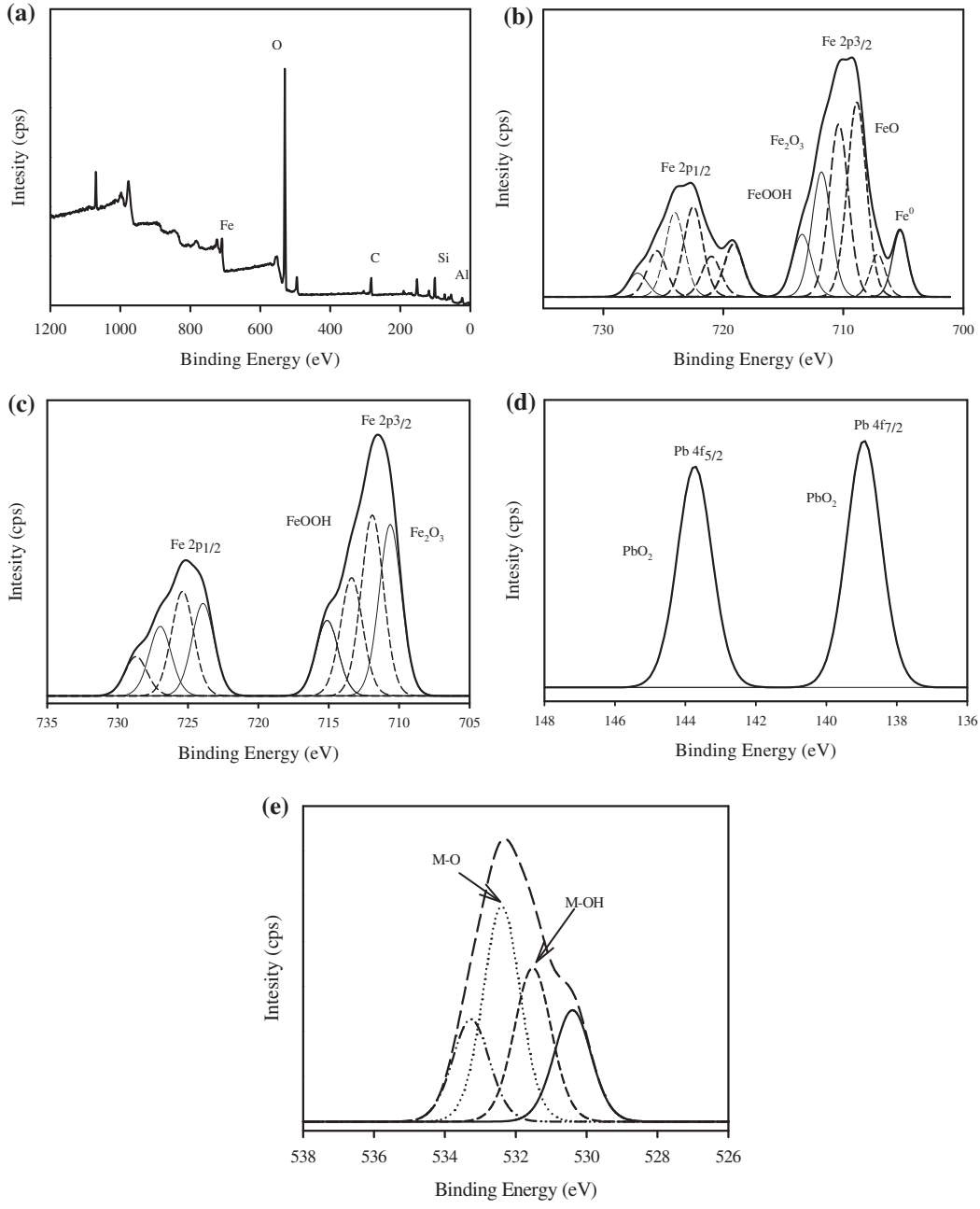

Fig. 7. XPS spectra of ZVI-D_2 adsorb with 1,000 ppm of Pb^{2+} at 60 min. (a) full survey of ZVI-D_2 before adsorption, (b) iron in ZVI-D_2 before adsorption, (c) iron in ZVI-D_2 after adsorption, (d) Pb^{2+} in ZVI-D_2 after adsorption, and (e) oxygen in ZVI-D_2 after adsorption.

indication that the process is endothermic (Fig. 6). A similar trend has been reported for the removal of cadmium by nano zero-valent iron particles [43]. Negative values of ΔG° indicate that spontaneous adsorption and the degree of spontaneity of the reaction increases with increasing temperatures [45]. It is clear that the free energy of lead adsorption on ZVI-D_2 is more negative at higher temperatures, which demonstrates that the spontaneity of the adsorption process increases with the rise in temperature. The ΔH° values were in the range of 15.26–47.11 kJ/mol with a mean value of 23.97 kJ/mol. The values conform to the endothermic nature of the adsorption process. The positive values of ΔS° were in the range of 61.00–155.37 J/mol K with a mean value of 87.30 J/mol K. The positive value of ΔS° suggests that the structural changes occur on the adsorbent and the unstructured solid/liquid interface in the adsorption system increases during the adsorption process which is similar to the research of Kul and Koyuncu [46], who studied the temperature-dependent adsorption of lead ion on diatomite. The results indicated that the adsorption process of lead ions onto ZVI-D_2 was spontaneous and endothermic in nature.

3.6. Mechanism of lead adsorption on ZVI-D_2

In order to identify the phases on ZVI-D_2 before and after adsorption, untreated ZVI-D_2 and 1 g of ZVI-D_2 was loaded into the solution with 1,000 ppm of Pb^{2+} and left for the reaction to take place for 60 min, were analyzed by the XPS. The XPS analysis of untreated ZVI-D_2 revealed that elementary elements in the ZVI-D_2 were at Fe 2p 709.1 eV, O 1s 530.1 eV, C 1s 283.1 eV, Si 2p 101.1 eV and Al 2p 73.1 eV, as shown in Fig. 7(a). The peaks at 705.3 eV correspond to zero-valent iron (Fe^0 $2p_{3/2}$), while 711.5 and 725.2 eV did to Fe $2p_{3/2}$ and Fe $2p_{1/2}$. The main iron species of ZVI-D_2 were Fe^0, Fe_2O_3, $Fe(OH)_3$, and FeOOH [47] as given in Fig. 7(b). It was confirmed that the outer shell structure of ZVI-D_2presented iron oxides and iron hydroxide consistent with research of X. Zhang et al. [25]. Through the binding energy analyzes, Si 2p peaks at 101.7 and 102.8 eV were assigned to the Si–O and Si–OH, respectively, while the Al 2p peaks at 73.4 and 74.6 eV were similarly assigned to AlOOH and $Al(OH)_3$, respectively.

For the treated ZVI-D_2, the peak corresponding to Fe^0 was not observed, while the XPS spectra showed Fe_2O_3 and FeOOH as the dominant energy peaks. This result indicated that Fe^0 can be severely oxidized to Fe_2O_3 and FeOOH, as shown in Fig. 7(c). Moreover, the result revealed that SiO_2 and $Al(OH)_3$ of diatomite structure became Si–O, Si–OH, AlOOH, and $Al(OH)_3$, respectively after lead adsorption because of oxidation reaction. In order to confirm the existence of lead on the surface of ZVI-D_2, the Pb $4f_{7/2}$ and Pb $4f_{5/2}$ narrow scans were illustrated in Fig. 7(d). From this figure, it could be seen that peaks occur at 138.9 and 143.7 eV, which indicate that $Pb(OH)_2$ and PbO exist on the surface [25,48]. Nevertheless, Pb^0 was not detected on the XPS data, but the XRD analysis confirmed the existence of Pb^0 [24] (Fig. 8), indicating that Pb^0 may be adsorbed into the core structure of Fe^0, and it may be deeper from the surface than the detection limitation of XPS analysis [49]. It is interesting to note that the peak ratio of the oxygen at 531.5 and 532.3 eV (Fig. 7(e)) increased after Pb^{2+} adsorption, suggesting that hydroxyl bonded to the metal groups (M–OH) and the metal oxide groups (M–O) [50,51] built on the surface of ZVI-D_2, which confirmed that the Pb^{2+} adsorbed on the surface of ZVI-D_2 in the form of $Pb(OH)_2$ and PbO. It can be concluded that Pb^0, $Pb(OH)_2$, and PbO exist on the surface of ZVI-D_2.

Based on the result of this study, mechanisms of Pb(II) adsorption onto ZVI-D_2 are thought to mainly depend on the type of active sites on the surface of adsorbent and the species of adsorbate. In this study, the initial pH of the solution was 5. Lead in the solution was mainly Pb^{2+}. Based upon the premise discussed above, the mechanism for Pb^{2+} removal on the ZVI-D_2 is proposed and presented in Fig. 9. The figure suggests two sections of the Pb^{2+}-ZVI-D_2 reactions. Section I: the Fe^0 is oxidized by water and oxygen, which is a natural corrosion reaction, to form Fe_2O_3 and FeOOH. Then, Pb^{2+} is reduced to Pb^0 by electrons donated from Fe^0 oxidations due to the standard reduction potential of Pb^{2+}/Pb^0 (−0.1263 V), which is greater than that of Fe^{2+}/Fe^0 (−0.4402 V) [52]. Section II: can be divided into 8 pathways. The Fe_2O_3, FeOH, and FeOOH can react with the Pb^{2+} to produce

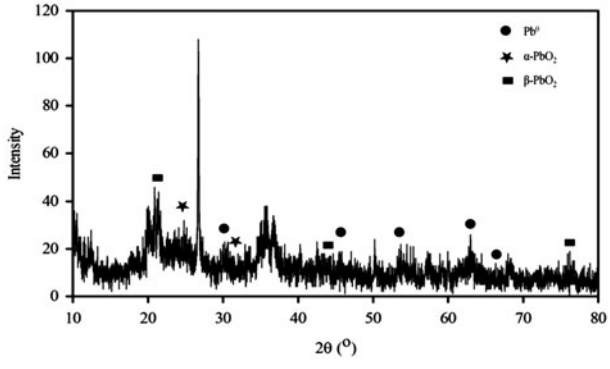

Fig. 8. XRD pattern of ZVI-D_2 adsorb with 1,000 ppm of lead ion at 60 min.

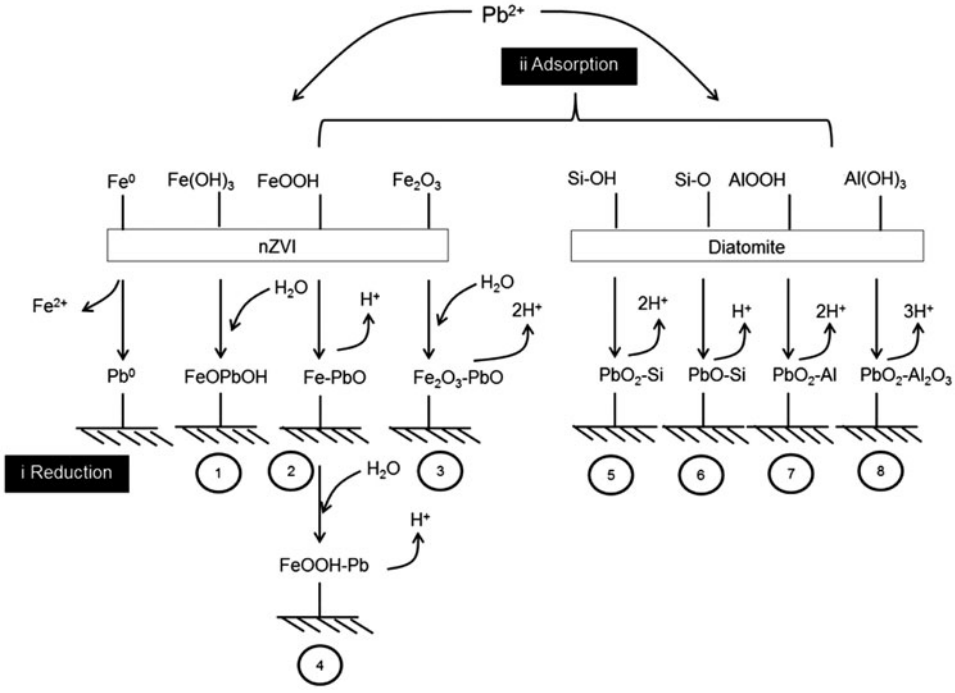

Fig. 9. The mechanism of adsorption lead ion from aqueous solution by using ZVI-D_2.

FeOPbOH, PbO-Fe, PbO_2-Fe_2O_3, and PbO-FeOOH (pathway 1–4). Pb^{2+} is adsorbed on the surface of diatomite which has Si–OH and Si–O to form the PbO_2–Si and PbO–Si, respectively (pathway 5–6), and Pb^{2+} can be adsorbed by the AlOOH and $Al(OH)_3$ in the diatomite structure to form $Pb(OH)_2$–Al and PbO_2–Al_2O_3 (pathway 7–8).

4. Conclusions

The principal finding of this research is that double coatings of diatomite with ZVI (ZVI-D_2) prove to be the most effective in removing lead in the solution. With the initial lead concentration of 100 ppm, 97.36% of lead was removed. Even though the result of XRD analysis did not reveal any phases of iron in ZVI-D_2, Fe^0, Fe_2O_3, $Fe(OH)_3$, and FeOOH were found on the surface of the diatomite by the XPS analysis. This is thought to be due to good dispersion of iron on the diatomite. By studying adsorption of lead on ZVI-D_2, it was found that the adsorption follows Langmuir model. The adsorption should be chemical adsorption. This is consistent with the mean adsorption energy of 54.78 kJ/mol obtained from the D–R model. The experimental results on adsorption kinetics revealed that the adsorption fitted well with the pseudo-second-order model with R^2 of 0.99. Furthermore, the use of intra-particle model indicated that the rate-controlling step is film diffusion and intra-particle diffusion.

The mechanism of lead adsorption by ZVI-D_2 can be explained with XPS and XRD analyses. It can be concluded that, after adsorption, three species of lead, namely, Pb^0, $Pb(OH)_2$, and PbO were found. It is therefore proposed that Pb^{2+} is reduced to Pb^0 by Fe^0, whereas, $Fe(OH)_3$, FeOOH, and Fe_2O_3 will react with Pb^{2+} to form FePbOH, Fe-PbO, and Fe_2O_3-PbO, respectively. Fe–PbO might also react with water to give FeOOH–Pb whereas Si–OH, Si–O, AlOOH, and $Al(OH)_3$ will react with Pb^{2+} to form PbO_2–Si, PbO–Si, PbO_2–Al, and PbO_2–Al_2O_3, respectively.

Acknowledgements

This research was financially supported by faculty of engineering KhonKaen University.

References

[1] C.J. Schmitt, W.G. Brumbaugh, T.W. May, Accumulation of metals in fish from lead–zinc mining areas of southeastern Missouri, USA, Ecotoxicol. Environ. Saf. 67 (2007) 14–30.
[2] X. Zhang, S. Lin, X.-Q. Lu, Z. Chen, Removal of Pb(II) from water using synthesized kaolin supported nanoscale zero-valent iron, Chem. Eng. J. 163 (2010) 243–248.

[3] A. Sarı, M. Tuzen, M. Soylak, Adsorption of Pb(II) and Cr(III) from aqueous solution on Celtek clay, J. Hazard. Mater. 144 (2007) 41–46.
[4] C. Dou, J. Zhang, Effects of lead on neurogenesis during zebrafish embryonic brain development, J. Hazard. Mater. 194 (2011) 277–282.
[5] WHO, Guidelines for drinking-water quality, fourth edition, WHO, (2011). Available from: <http://www.who.int/water_sanitation_health/publications/2011/dwq_guidelines/en/>, (accessed June 30, 2015).
[6] A. Sarı, M. Tuzen, Kinetic and equilibrium studies of Pb(II) and Cd(II) removal from aqueous solution onto colemanite ore waste, Desalination 249 (2009) 260–266.
[7] A. Naeem, M.T. Saddique, S. Mustafa, Y. Kim, B. Dilara, Cation exchange removal of Pb from aqueous solution by sorption onto NiO, J. Hazard. Mater. 168 (2009) 364–368.
[8] H.-P. Chao, C.-C. Chang, Adsorption of copper(II), cadmium(II), nickel(II) and lead(II) from aqueous solution using biosorbents, Adsorption 18 (2012) 395–401.
[9] H. Bessbousse, T. Rhlalou, J.-F. Verchère, L. Lebrun, Removal of heavy metal ions from aqueous solutions by filtration with a novel complexing membrane containing poly(ethyleneimine) in a poly(vinyl alcohol) matrix, J. Membr. Sci. 307 (2008) 249–259.
[10] S. Kundu, A.K. Gupta, Adsorption characteristics of As(III) from aqueous solution on iron oxide coated cement (IOCC), J. Hazard. Mater. 142 (2007) 97–104.
[11] M.S.H. Mak, P. Rao, I.M.C. Lo, Zero-valent iron and iron oxide-coated sand as a combination for removal of co-present chromate and arsenate from groundwater with humic acid, Environ. Pollut. 159 (2011) 377–382.
[12] S.M. Ponder, J.G. Darab, J. Bucher, D. Caulder, I. Craig, L. Davis, N. Edelstein, W. Lukens, H. Nitsche, L. Rao, D.K. Shuh, T.E. Mallouk, Surface chemistry and electrochemistry of supported zerovalent iron nanoparticles in the remediation of aqueous metal contaminants, Chem. Mater. 13 (2001) 479–486.
[13] X. Li, D.W. Elliott, W. Zhang, Zero-valent iron nanoparticles for abatement of environmental pollutants: Materials and engineering aspects, Crit. Rev. Solid State Mater. Sci. 31 (2006) 111–122.
[14] X. Dou, R. Li, B. Zhao, W. Liang, Arsenate removal from water by zero-valent iron/activated carbon galvanic couples, J. Hazard. Mater. 182 (2010) 108–114.
[15] S.A. Kim, S. Kamala-Kannan, K.-J. Lee, Y.-J. Park, P.J. Shea, W.-H. Lee, H.-M. Kim, B.-T. Oha, Removal of Pb (II) from aqueous solution by a zeolite–nanoscale zero-valent iron composite, Chem. Eng. J. 217 (2013) 54–60.
[16] Y.-F. Pan, C.T. Chiou, T.-F. Lin, Adsorption of arsenic (V) by iron-oxide-coated diatomite (IOCD), Environ. Sci. Pollut. Res. 17 (2010) 1401–1410.
[17] Y. Zhang, Y. Li, J. Li, L. Hu, X. Zheng, Enhanced removal of nitrate by a novel composite: Nanoscale zero valent iron supported on pillared clay, Chem. Eng. J. 171 (2011) 526–531.
[18] G. Sheng, S. Wang, J. Hu, Y. Lu, J. Li, Y. Dong, X. Wang, Adsorption of Pb(II) on diatomite as affected via aqueous solution chemistry and temperature, Colloids Surf., A: Physicochem. Eng. Aspects 339 (2009) 159–166.
[19] R. Köseoglu, F. Köksal, E. Çiftci, M. Akkurt, Identification of paramagnetic radicals in γ-irradiated natural diatomite minerals by electron paramagnetic resonance, J. Mol. Struct. 733 (2005) 151–154.
[20] E. Eren, Removal of lead ions by Unye (Turkey) bentonite in iron and magnesium oxide-coated forms, J. Hazard. Mater. 165 (2009) 63–70.
[21] M. Momčilović, M. Purenović, A. Bojić, A. Zarubica, M. Ranđelović, Removal of lead(II) ions from aqueous solutions by adsorption onto pine cone activated carbon, Desalination 276 (2011) 53–59.
[22] K. Wantala, S. Sthiannopkao, B. Srinameb, N. Grisdanurak, K.-W. Kim, S. Han, Arsenic adsorption by Fe Loaded on RH-MCM-41 synthesized from rice husk silica, J. Environ. Eng. 138 (2012) 119–128.
[23] M.D.G. de Luna, K.K.P. Rivera, T. Suwannaruang, K. Wantala, Alachlorphotocatalytic degradation over uncalcined Fe–TiO_2 loaded on granular activated carbon under UV and visible light irradiation, Desalin. Water Treat. (2015) 1–11.
[24] N. Caliskan, A.R. Kul, S. Alkan, E.G. Sogut, İ. Alacabey, Adsorption of Zinc(II) on diatomite and manganese-oxide-modified diatomite: A kinetic and equilibrium study, J. Hazard. Mater. 193 (2011) 27–36.
[25] X. Zhang, S. Lin, Z. Chen, M. Megharaj, R. Naidu, Kaolinite-supported nanoscale zero-valent iron for removal of Pb^{2+} from aqueous solution: Reactivity, characterization and mechanism, Water Res. 45 (2011) 3481–3488.
[26] J. Hu, I.M.C. Lo, G. Chen, Performance and mechanism of chromate(VI) adsorption by δ-FeOOH-coated maghemite (γ-Fe_2O_3) nanoparticles, Sep. Purif. Technol. 58 (2007) 76–82.
[27] N. Arancibia-Miranda, S.E. Baltazar, A. García, A.H. Romero, M.A. Rubio, D. Altbir, Lead removal by nano-scale zero valent iron: Surface analysis and pH effect, Mater. Res. Bull. 59 (2014) 341–348.
[28] M. Irani, M. Amjadi, M.A. Mousavian, Comparative study of lead sorption onto natural perlite, dolomite and diatomite, Chem. Eng. J. 178 (2011) 317–323.
[29] J.U.K. Oubagaranadin, Z.V.P. Murthy, Adsorption of divalent lead on a montmorillonite−illite type of clay, Ind. Eng. Chem. Res. 48 (2009) 10627–10636.
[30] H. Abdel-Samad, P.R. Watson, An XPS study of the adsorption of lead on goethite (α-FeOOH), Appl. Surf. Sci. 136 (1998) 46–54.
[31] H. Zhu, Y. Jia, X. Wu, H. Wang, Removal of arsenic from water by supported nano zero-valent iron on activated carbon, J. Hazard. Mater. 172 (2009) 1591–1596.
[32] P.C. Mishra, R.K. Patel, Removal of lead and zinc ions from water by low cost adsorbents, J. Hazard. Mater. 168 (2009) 319–325.
[33] M.A.M. Khraisheh, Y.S. Al-degs, W.A.M. Mcminn, Remediation of wastewater containing heavy metals using raw and modified diatomite, Chem. Eng. J. 99 (2004) 177–184.
[34] J.C. Igwe, A.A. Abia, Adsorption isotherm studies of Cd(II), Pb(II) and Zn(II) ions bioremediation from aqueous solution using unmodified and EDTA-modified maize cob, EcléticaQuím 32 (2007) 33–42.
[35] S. Karagoz, T. Tay, S. Ucar, M. Erdem, Activated carbons from waste biomass by sulfuric acid activation and their use on methylene blue adsorption, Bioresour. Technol. 99 (2008) 6214–6222.

[36] B.H. Hameed, D.K. Mahmoud, A.L. Ahmad, Equilibrium modeling and kinetic studies on the adsorption of basic dye by a low-cost adsorbent: Coconut (*Cocos nucifera*) bunch waste, J. Hazard. Mater. 158 (2008) 65–72.
[37] A. Sarı, M. Tuzen, D. Cıtak, M. Soylak, Adsorption characteristics of Cu(II) and Pb(II) onto expanded perlite from aqueous solution, J. Hazard. Mater. 148 (2007) 387–394.
[38] M.-C. Shih, Kinetics of the batch adsorption of methylene blue from aqueous solutions onto rice husk: Effect of acid-modified process and dye concentration, Desalin. Water Treat. 37 (2012) 200–214.
[39] W.H. Cheung, Y.S. Szeto, G. McKay, Intraparticle diffusion processes during acid dye adsorption onto chitosan, Bioresour. Technol. 98 (2007) 2897–2904.
[40] M. Özacar, İ.A. Şengil, H. Türkmenler, Equilibrium and kinetic data, and adsorption mechanism for adsorption of lead onto valonia tannin resin, Chem. Eng. J. 143 (2008) 32–42.
[41] B.H. Hameed, M.I. El-Khaiary, Sorption kinetics and isotherm studies of a cationic dye using agricultural waste: Broad bean peels, J. Hazard. Mater. 154 (2008) 639–648.
[42] M. Belhachemi, F. Addoun, Adsorption of congo red onto activated carbons having different surface properties: Studies of kinetics and adsorption equilibrium, Desalin. Water Treat. 37 (2012) 122–129.
[43] H.K. Boparai, M. Joseph, D.M. O'Carroll, Kinetics and thermodynamics of cadmium ion removal by adsorption onto nano zerovalent iron particles, J. Hazard. Mater. 186 (2011) 458–465.
[44] E.I. Unuabonah, K.O. Adebowale, B.I. Olu-Owolabi, Kinetic and thermodynamic studies of the adsorption of lead(II) ions onto phosphate-modified kaolinite clay, J. Hazard. Mater. 144 (2007) 386–395.
[45] M.T. Sulak, H.C. Yatmaz, Removal of textile dyes from aqueous solutions with eco-friendly biosorbent, Desalin. Water Treat. 37 (2012) 169–177.
[46] A.R. Kul, H. Koyuncu, Adsorption of Pb(II) ions from aqueous solution by native and activated bentonite: Kinetic, equilibrium and thermodynamic study, J. Hazard. Mater. 179 (2010) 332–339.
[47] A.A. Hermas, XPS analysis of the passive film formed on austenitic stainless steel coated with conductive polymer, Corros. Sci. 50 (2008) 2498–2505.
[48] Z. Özlem Kocabaş-Ataklı, Y. Yürüm, Synthesis and characterization of anatase nanoadsorbent and application in removal of lead, copper and arsenic from water, Chem. Eng. J. 225 (2013) 625–635.
[49] H. Woo, J. Park, S. Lee, S. Lee, Effects of washing solution and drying condition on reactivity of nanoscale zero valent irons (nZVIs) synthesized by borohydride reduction, Chemosphere 97 (2014) 146–152.
[50] A. Mekki, D. Holland, C.F. McConville, M. Salim, An XPS study of iron sodium silicate glass surfaces, J. Non-Cryst. Solids 208 (1996) 267–276.
[51] K. Artyushkova, S. Levendosky, P. Atanassov, J. Fulghum, XPS structural studies of nano-composite non-platinum electrocatalysts for polymer electrolyte fuel cells, Top. Catal. 46 (2007) 263–275.
[52] Y. Xi, M. Mallavarapu, R. Naidu, Reduction and adsorption of Pb^{2+} in aqueous solution by nano-zero-valent iron—A SEM, TEM and XPS study, Mater. Res. Bull. 45 (2010) 1361–1367.